Geophysical Research Letters

RESEARCH LETTER
10.1029/2018GL078286

Key Points:
- The production of vent discharges is tightly coupled to the compressible fluid dynamics associated with individual volcanic explosions
- The supersonic (Prandtl-Meyer) expansion of an overpressured jet controls the location and timing of vent discharges
- The magnitude of the vent overpressure, as well as the structure of an overpressured jet, can be inferred from the location of vent discharges

Correspondence to:
J. S. Méndez Harper,
joshua.mendez@emory.edu

Citation:
Méndez Harper, J. S., Cimarelli, C., Dufek, J., Gaudin, D., & Thomas, R. J. (2018). Inferring compressible fluid dynamics from vent discharges during volcanic eruptions. *Geophysical Research Letters*, *45*. https://doi.org/10.1029/2018GL078286

Received 9 APR 2018
Accepted 26 JUN 2018
Accepted article online 5 JUL 2018

Inferring Compressible Fluid Dynamics From Vent Discharges During Volcanic Eruptions

J. S. Méndez Harper[1,2], C. Cimarelli[3], J. Dufek[1], D. Gaudin[3], and R. J. Thomas[4]

[1]School of Earth and Atmospheric Sciences, Georgia Institute of Technology, Atlanta, GA, USA, [2]School of Electrical and Computer Engineering, Georgia Institute of Technology, Atlanta, GA, USA, [3]Department of Earth and Environmental Sciences, Ludwig-Maximilians-Universität, München, Germany, [4]Department of Electrical Engineering, New Mexico Institute of Mining and Technology, Socorro, NM, USA

Abstract Observations at numerous volcanoes reveal that eruptions are often accompanied by continual radio frequency (CRF) emissions. The source of this radiation, however, has remained elusive until now. Through experiments and the analysis of field data, we show that CRF originates from proximal discharges driven by the compressible fluid dynamics associated with individual volcanic explosions. Blasts produce flows that expand supersonically, generating regions of weakened dielectric strength in close proximity to the vent. As erupted material—charged through fragmentation, friction, or other electrification process—transits through such a region, pyroclasts remove charge from their surfaces in the form of small interparticle spark discharges or corona discharge. Discharge is maintained as long as overpressured conditions at the vent remain. Beyond describing the mechanism underlying CRF, we demonstrate that the magnitude of the overpressure at the vent as well as the structure of the supersonic jet can be inferred in real time by detecting and locating CRF sources.

1. Introduction

Volcanic eruptions often display a range of electrostatic processes, including anomalous electric fields and spectacular lightning displays (Aizawa et al., 2016; Behnke et al., 2013; Behnke & Bruning, 2015; Cimarelli et al., 2016; Gilbert et al., 1991; Lane & Gilbert, 1992; Miura et al., 2002; Woodhouse & Behnke, 2014). Although the underlying microphysics of ash electrification are not fully understood, recent field campaigns have revealed that electrical phenomena are intimately related to eruptive hydrodynamics (Behnke & Bruning, 2015; Cimarelli et al., 2016, 2016; Van Eaton et al., 2016). Understanding these connections remains a prominent goal in volcanology because electrical activity emits radiation that can be monitored remotely. Thus, if well characterized, these signals may serve to probe the internal, obscured dynamics of eruptive events in manners that have not been achieved previously. For instance, observations during the Augustine (2006) and Redoubt (2009) eruptions suggest that electrostatic processes coevolve with changes in flow behavior (Behnke & Bruning, 2015; Behnke et al., 2018, 2013; Smith et al., 2018; Thomas et al., 2007). In particular, both Alaskan volcanoes produced two distinct electrical behaviors during their eruptions: (1) initial, quasi-continual radio frequency (RF) outbursts associated with individual explosions followed by (2) more intermittent, although more spatially extensive, spark discharges in maturing plumes. The latter modality, comprising *near-vent* and *plume lightning*, typically generates brilliant flashes several hundreds of meters to kilometers in length and emits impulsive RF signals (Figure 1a; Thomas et al., 2007). These spark discharges occur anywhere between a few hundreds of meters above the vent to kilometers away in the distal plume. Because of their conspicuous nature and similarity to thundercloud lightning, both near-vent and plume lightning have been the focus of the most recent studies of electrostatic phenomena at volcanoes (Aizawa et al., 2016; Cimarelli et al., 2016; Nicora et al., 2013; Van Eaton et al., 2016).

Contrastingly, the first discharge modality, referred to as *vent discharges* (sometimes, vent lightning), is more obscure. Revealing themselves en masse as a continual RF (CRF) or persistent RF "hum" at a distance, vent discharges have been inferred to be small, visually inappreciable sparks occurring between individual ash particles or small clusters of particles in the flow (Behnke et al., 2013, 2018; Thomas et al., 2007). Such discharges occur at or just above the volcanic vent and occur in tempo with discrete explosions (Figure 1a). Interestingly, the RF energy emitted by vent discharges has been shown to increase with the magnitude of overpressure at the vent for a given explosion (Behnke et al., 2013; Behnke & Bruning, 2015).

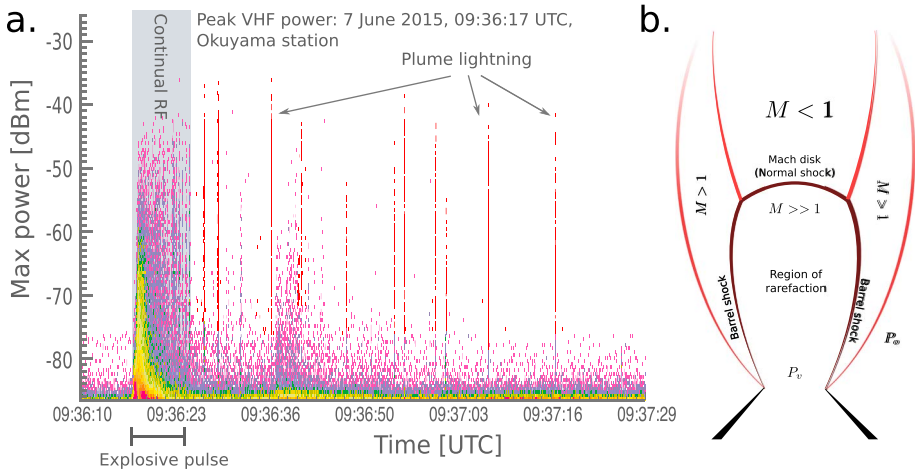

Figure 1. Electrical activity during the 2015 eruption of Sakurajima and the structure of an underexpanded jet. (a) Data collected with a Lightning Mapping Array during a 15 June eruption at Sakurajima (Behnke et al., 2018) showing the spectral differences between vent and plume lightning. While plume lightning manifests itself as discrete, impulsive signals (red, vertical lines), vent activity appears as a "continual" signal rising from the noise floor. As can be seen, continual radio frequency correlates temporally with the duration of an explosive event (gray shaded area). Figure modified from Behnke et al., 2018. (b) Schematic structure of an underexpanded jet, showing the region of rarefaction between the vent and the normal shock, contained within a barrel shock.

The small length scales (likely, centimeters to a few meters) and high rates (up to several dozen events per millisecond) associated with vent discharges hint that the volumetric charge density in proximal volcanic jets may be as much as an order of magnitude larger than that found in thunderclouds or distal plume regions (Aizawa et al., 2016; McNutt & Williams, 2010). This is an unsurprising observation given that explosions likely generate large amounts of charge per unit surface area through elevated rates of fractoelectric and triboelectric charging (James et al., 2000; Méndez Harper et al., 2015; Méndez Harper & Dufek, 2016). Indeed, proximal discharges could reflect conventional or dielectric breakdown processes (Aizawa et al., 2016), rather than the more complex processes thought to operate in thunderclouds (Dwyer, 2005; Dwyer & Uman, 2014; Gurevich et al., 1992). Furthermore, unlike near-vent and plume discharges, vent discharges do not seem to require large-scale charge separation and do not importantly modify ambient electric fields as measured from the ground (Behnke et al., 2018). Together, these characteristics—the timing of discharges, their small length scales, and their confinement to regions directly adjacent to the vent—may suggest that this electrical activity directly reflects explosive processes at the volcanic source. However, a physical mechanism linking explosive processes to electrostatic phenomena has not been described until now. Here we show that vent discharges are driven by supersonic expansion processes associated with powerful explosions. Indeed, our works demonstrate that the compressible fluid dynamics describing overpressured jets has the ability to finely tune the breakdown strength of a gas carrying charged particles, placing strict temporal and spatial limits on the occurrence of proximal discharges.

2. Model

The energetic volcanic explosions that produce vent discharges are often also associated with flows that are *overpressurized* or *underexpanded* and supersonic (Kieffer, 1981; Ogden et al., 2008; Orescanin et al., 2010). Such conditions occur when the pressure at the vent is higher than ambient by at least a factor of 2 (Orescanin et al., 2010). Upon emerging from the conduit, the jet undergoes Prandtl-Meyer expansion to form a barrel shock structure (Figure 1b). With increasing distance from the vent, the flow accelerates to elevated Mach numbers and decreases rapidly in both density and pressure (Kieffer, 1981; Ogden et al., 2008; Orescanin et al., 2010; Orescanin & Austin, 2010). This pressure drop with distance from an underexpanded nozzle has been described in detail by Owen and Thornhill (1948) and Adamson and Nicholls (1959) using the method of characteristics (The analysis of the pressure variation in volcanic jets explored here makes

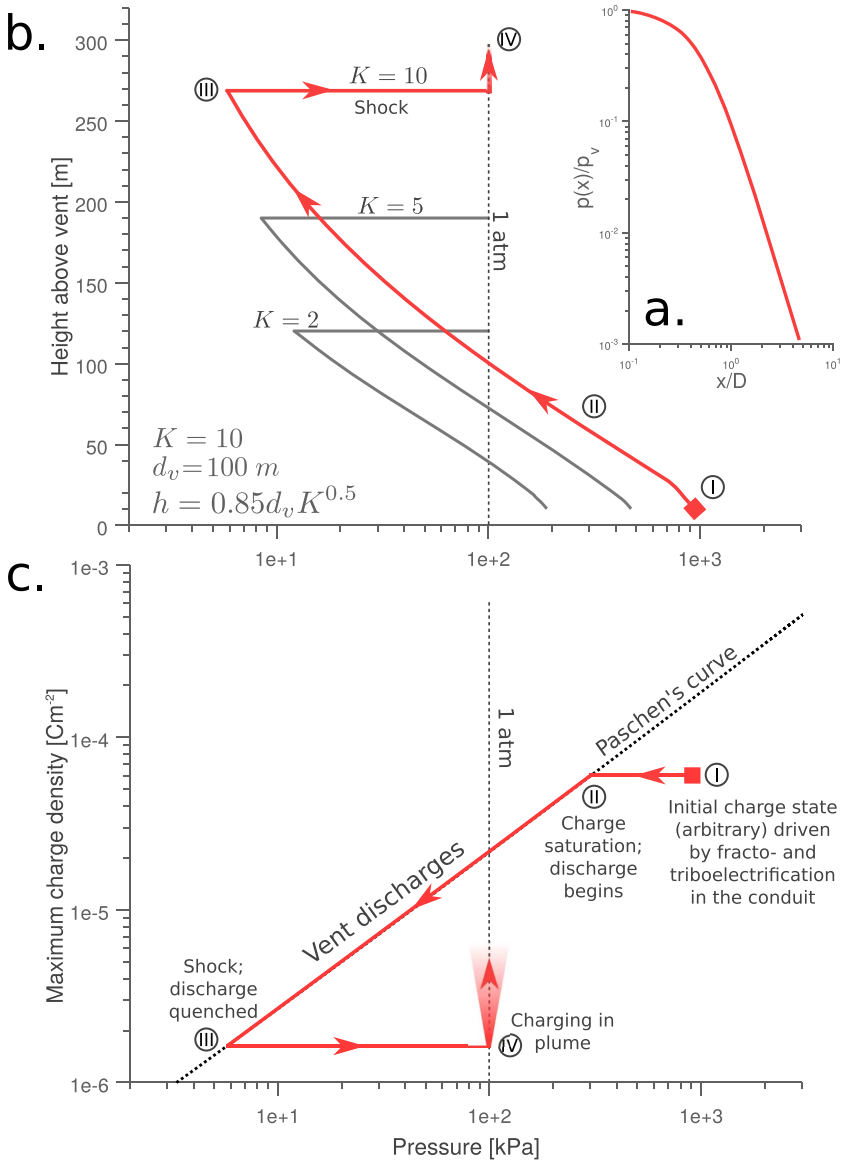

Figure 2. Variation in pressure within the underexpanded jet and associated electrostatic effects. (a) Normalized pressure variation along the centerline of the jet as a function of distance normalized by the vent diameter (modified from Owen & Thornhill, 1948). (b) The pressure variation in a jet as function of altitude for three different *K* factors, 2, 5, 10, for d_v = 100 and *C* = 0.85. Note rarefaction during the expansion and the stepwise recompression at the shock. (c) The proposed discharge mechanism in a jet with *K* = 10. A grain at high pressure starts off undersaturated in charge (Point I). As the pressure in the jet drops during expansion, the ability of the gas to hold charge is also diminished. At some point, the potential on the particle intersects the Paschen curve and discharge is initiated (Point II). Charge loss (and the production of CRF) continues as long as the pressure continues to drop. At the shock, the pressure rapidly climbs and discharge is cut off (Point III). Subsequent charging is due to electrification in the plume (Point IV).

use of their numerical models [Figure 2a]). Indeed, the pressure in the expanding flow may drop below atmospheric by up to one or two orders of magnitude (Ogden et al., 2008; Orescanin et al., 2010; Orescanin & Austin, 2010). At some distance, however, this rarefaction terminates abruptly in a normal shock (Mach disk). There, the flow becomes subsonic and a sudden increase in pressure and density takes places. The position of the shock has been shown to be function of the vent diameter, d_v, as well as the overpressure factor, $K = P_v/P_o$ (where P_v is the pressure at the vent and P_o is the atmospheric pressure).

Under a pseudo-gas approximation relevant to volcanic eruptions, the elevation (or the distance from the vent) of the Mach disk is given by Ogden et al. (2008):

$$h = Cd_V K^{\alpha}. \tag{1}$$

For jets sourced from large pressurized (infinite) reservoirs, C takes values ranging between 0.67 (Orescanin et al., 2010) and 0.85 (Ogden et al., 2008), and $\alpha = 0.5$. For finite reservoirs with overpressure factors smaller than 15, experimental work suggests that C is closer to 0.41 and $\alpha = 0.66$ (Orescanin & Austin, 2010). While details of this model may change as the pseudo-gas assumption is relaxed, the general form of this relationship should remain valid. Indeed, the number of fine-grained particles available in most volcanic eruptions suggests that this expression is likely appropriate for many scenarios (Kieffer & Sturtevant, 1984; Pelanti & LeVeque, 2006).

For demonstrative purposes, consider three jets described by $C = 0.85$, $d_v = 100$ m, and $K = 2, 5, 10$. As rendered in Figure 2b, the pressure in the jets drops with distance from the vent until the flow crosses the normal shock. At the Mach disk, the pressure returns to a value near atmospheric (although this may continue to oscillate downstream of the shock). This rarefaction and sudden recompression have important consequences for breakdown processes. According to Paschen's Law, the maximum electric field, E_b, that can be sustained between two charged surfaces, separated by some distance d, before the intervening gas undergoes electrical breakdown is roughly inversely proportional to pressure (for pressures of up to 13–20 atmospheres; Cohen, 1956; Paschen, 1889). Quantitatively, such relationship can be expressed as

$$E_b = \frac{Bp}{\ln\left(\frac{Apd}{\ln(1/\gamma+1)}\right)}. \tag{2}$$

Above, p is the pressure, γ is the second Townsend coefficient (10^{-2}), and B and A are constants with values of 1.14×10^4 kPa^{-1} m^{-1} and 2.77×10^5 VkPa^{-1} m^{-1}, respectively (Helling et al., 2013; Sentman, 2004). From the breakdown field, the maximum charge densities on the two surfaces can then be computed as

$$Q/A_{max} = \in_r \in_o E_b, \tag{3}$$

where $\in_r$ is the relative permittivity of the gas and $\in_o$ is the permittivity of free space (Hamamoto et al., 1992; Helling et al., 2013). For conditions at sea level, two charged surfaces separated by a distance of 1 m would require charge densities on the order 10^{-5} Cm^{-2} to produce breakdown (this corresponds to an electric field of 3 MVm^{-1}). At 5 km above sea level, however, the same two surfaces could only sustain a charge density about half this value (Dwyer, 2005; Dwyer & Uman, 2014; Marshall et al., 1995). We note that some experimental data suggest that the maximum charge that can be sustained on a particle increases with decreasing particle size (Hamamoto et al., 1992). However, because the behavior of equations (2) and (3) will remain the same (i.e., a decrease in dielectric strength with decreasing pressure), we neglect size effects in the present work.

In the context of volcanic jets, the charged surfaces in equation (3) are either the surfaces of individual electrified pyroclasts (ash particles) or the "boundaries" of regions of charged grains concentrated through gravitational or hydrodynamic processes. As these surfaces are advected between the vent and Mach disk, the pressure of the gas surrounding them decreases and, with it, the breakdown strength of the gas. As we have said, however, rarefaction does not proceed indefinitely and there is stepwise jump in pressure at the Mach disk. There, a corresponding increase in the breakdown strength occurs. Continuing the analysis of the jets rendered in Figure 2b, the effects of pressure on the insulating properties of the jet can be assessed in Figure 2c. In that figure, we track the theoretical maximum charge densities on grain surfaces carried by a hypothetical overpressured jet with K = 10. At the vent, where the pressure is 10 times that of atmospheric, the maximum charge density that can be sustained on a particle is ~10^{-4} Cm^{-2} (assuming charged surfaces are separated by ~1 m—this value would be lower for more concentrated flows; Cross, 1987). For argument's sake, however, assume that charging mechanisms in the conduit are not completely efficient and ash particles emerge from the vent in slightly undersaturated conditions (point I in Figure 2c). Because the charge density at this point is below the Paschen limit (black, dotted line), grains are electrostatically stable. They

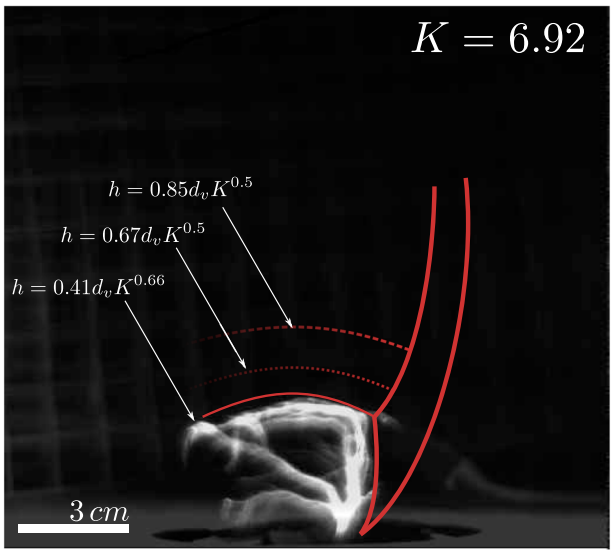

Figure 3. An experimental visualization of vent discharges. Composite image showing the tortuous path of discharges near the vent. Because of the increasingly weak dielectric strength of the gas away from the vent up until the Mach disk, discharges remain confined to the barrel shock. Maximum overpressure conditions for this flow were $K = 6.92$, $d_v = 2.8$ cm. Horizontal red curves in photo were computed using equation (1). Vertical curves are purely schematic in nature.

do not lose charge. However, as the jet expands and the pressure drops, the ability of the atmosphere to retain charge depreciates. At some pressure (point II in Figure 2c), the charge density on particles intersects Paschen's curve. Here charged surfaces find themselves in charge-saturated conditions. Any further reduction in pressure results in discharge to keep the charge density just below the Paschen limit. Discharge may occur between two adjacent particles (or particle collections) or directly to the atmosphere as corona or partial discharge. Discharge is maintained as long as the pressure in the jet continues to drop. Note that higher overpressures at the vent lead to deeper pressure undershoots and require ash surfaces to shed larger amounts of charge (Figure 2). Upon reaching the shock, the pressure in the jet increases precipitously. Charge loss is abruptly cut off as the Paschen limit jumps well above the potentials associated with the charge-depleted grains (point III). The shock effectively quenches the discharge. Past the Mach disk, grains may again collect charge as they undergo particle-particle collisions or as other electrification mechanism become active (point IV; Arason et al., 2011; McNutt & Williams, 2010). Compression/expansion waves exist downstream of the first normal shock, leading to additional shock cells in the jet. Thus, the maximum dielectric strength of the gas may continue to vary as pressure changes within these structures. However, these pressure fluctuations are likely to be less prominent than those in the first barrel shock (Ogden et al., 2008).

3. Experiments and Results

According to the model above, the Mach disk represents a sharp transition between a region of low dielectric strength (prior to the Mach disk) and one of high breakdown strength (past the Mach disk) within the flow. Thus, one would expect most electrical discharges to occur within the rarefied region upstream of the shock, with little activity in the denser downstream flow. We tested this hypothesis using a shock tube apparatus described extensively in previous work (Alidibirov & Dingwell, 2000, 1996; Cimarelli et al., 2014; Kueppers et al., 2006). The setup consists of a vertical autoclave capable of holding approximately 150 cm^3 of ash up to a pressure of 10 MPa (argon gas). Exceeding this pressure ruptures a set of copper diaphragms, ejecting the granular material from the tube by explosive decompression through a 2.8-cm nozzle into a low-pressure reservoir. As shown in Cimarelli et al. (2014), the venting produces a supersonic jet with abounding electrical discharges (likely a result of triboelectric and fractoelectric processes) with scales similar to those proposed for CRF sources (Figures 3 and 4c). Furthermore, Méndez Harper (2017) showed that the decompression event produces charged particles with charge densities comparable to those reported in field studies and other experiment endeavors. We tracked these spark discharges in the flow with a high-speed camera sampling at 36,000 fps. Discharges were also detected electrically by an electrostatic ring placed a few millimeters above the nozzle and connected to a high-speed data acquisition unit. In addition, the pressure at the vent was monitored throughout the experiment, allowing us to infer the geometry of the underexpanded jets using equation (1). The granular material employed in these experiments was commercially-processed pumice (from the Laascher See volcano in Germany) with a nominal grain size of 90–300 μm.

In accordance with the theoretical framework previously described, we find that discharges overwhelmingly occur within the region between the vent and the normal shock where the gas is rarefied (Figures 3 and 4). Indeed, some discharge channels appear to outline the boundaries of the barrel shock (Figure 3). Such behavior is unsurprising given that the least insulating regions in the jet structure exist immediately upstream of the Mach disk (see Figure 2). Comparatively, the region above the normal shock is strikingly devoid of electrical discharges. This paucity results from the fact that a significant portion of the charge on grain surfaces is lost within the barrel-shock structure. Thus, whatever surface charges survive the transit across normal shock are likely to be too few in number to produce electric fields capable of contending with the increased dielectric strength in overlying repressurized subsonic flow. In Figure 3, note that the extent of electrical discharges agree best geometrically with the volume of rarefaction when the elevation of the Mach disk (equation (1)) is

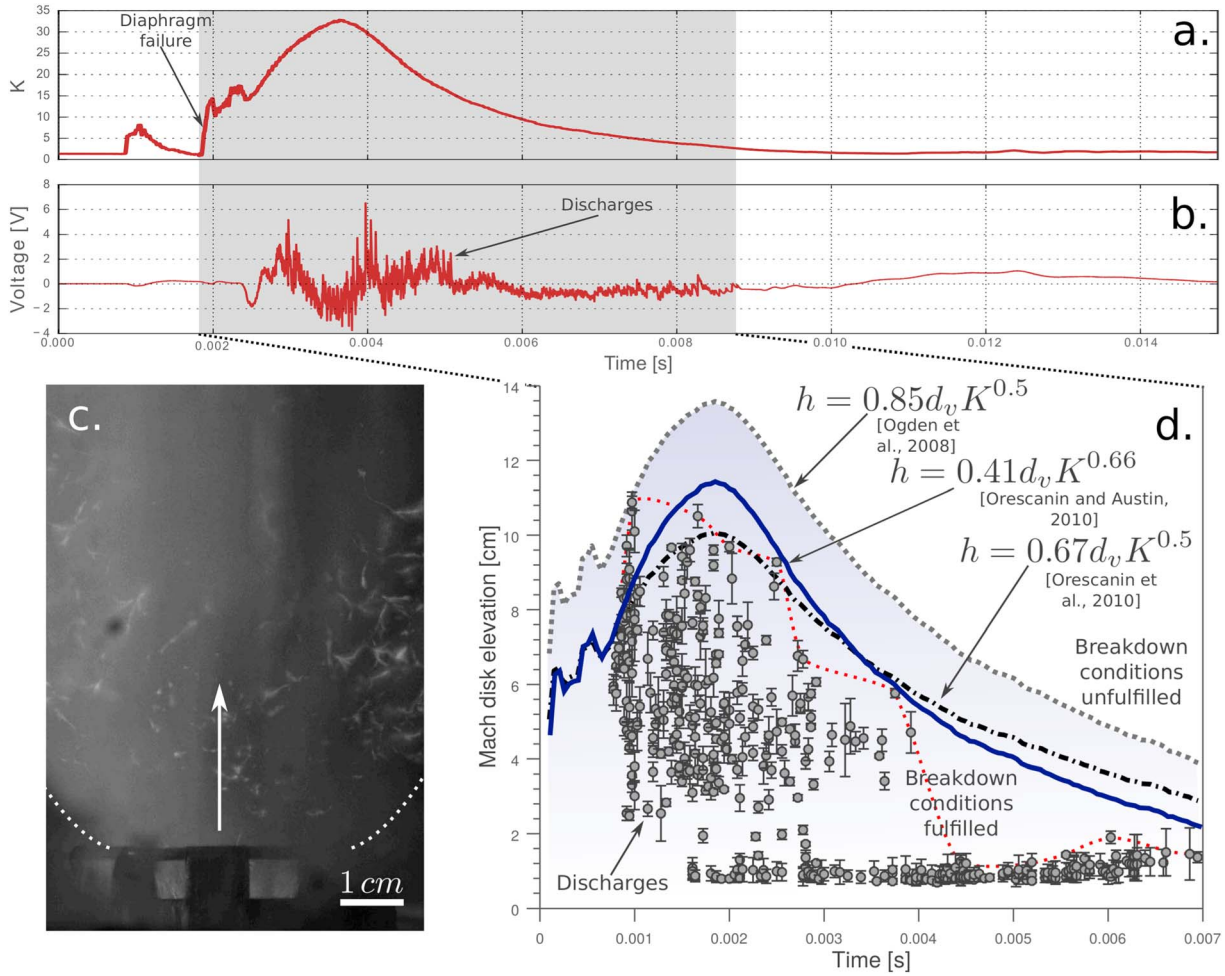

Figure 4. Inferring the dynamics of a supersonic jet from electrostatic discharges. (a) Overpressure factor, *K*, at the vent during a shock-tube experiment. (b) Discharges as recorded by the electrostatic ring sensors as high-frequency pulses. Note that discharges appear only when overpressures exist at the vent. (c) Time-lapse photograph (~6 ms) of all discharges observed in the scaled jet emanating from a 2.8-cm nozzle. (d) Location of discharges in the underexpanded jet as a function of time. Overwhelmingly, discharges remain in the region bounded between the vent (at $y = 0$ cm) and the normal shock (solid or dotted lines) because this area satisfies the conventional breakdown criteria. Red dotted line is the envelope of the data. As the shock structure collapses, the elevation of discharges also decreases. Discharges are extinguished as the overpressure factor approaches $K = 2$.

described by $C = 0.41$ and $\alpha = 0.66$ (Orescanin et al., 2010; Orescanin & Austin, 2010). That these parameters provide the best fit for the experimental data is to be expected given that they characterize supersonic jets emanating from a finite reservoir.

As described previously (Cimarelli et al., 2014), discharges in our experiments are only present while these overpressure conditions are maintained (Figures 4a and 4b). Because the flow is sourced from a small vessel, the overpressure at the vent rapidly decreases with time. The decrease in overpressure at the vent causes the volume of rarefaction (and the Mach disk) to ultimately retreat toward the vent. The reduction in size of the barrel shock is reflected by the spatial extent of discharges in the experiments—the volume supporting discharges in the flow also shrinks with time. This process can be seen in Figure 4c, where the locations of discharges with time (derived from the high-speed camera recordings) have been plotted together with the elevation of the normal shock as computed by equation (1) (for different values of C and α). For better comparison with the analytical solutions, the low-frequency envelope of the camera data is also plotted in Figure 4c (dotted, red curve). With exception of an initial transient at the onset of the experiment (possibly due to the pressure variations associated with the traveling shock when the diaphragms rupture), discharges are otherwise located bellow the Mach disk height predicted by equation (1) for the various values of C and α.

However, again, $h = 0.41 d_v K^{0.66}$, the mathematical expression for a finite reservoir, agrees best with our experimental data. Note that as the shock structure disappears (when K ~ 2), electrical activity ceases completely. The fact that discharges track area of rarefaction (and, consequently, the elevation of the normal shock) is of particular interest. If the extent of the electrical activity in the jet can be used to infer the position of the Mach disk in real time, these can also be used, in principle, to extract the overpressure conditions at the vent, thus allowing for refined evaluations of source conditions during an eruption.

4. Field Observations

Only recently has CRF been studied in detail at volcanoes. Yet the existing data show that the relationship between compressible flow dynamics and electrostatic processes observed in our experiments holds a clear counterpart in nature. During eruptions at Augustine (Thomas et al., 2007), Redoubt (Behnke et al., 2013; Behnke & Bruning, 2015), and Sakurajima (Behnke et al., 2018), electrical activity has been monitored using Lightning Mapping Array (LMA) sensors—devices that measure VHF radiation from atmospheric discharges. Because radio frequencies (unlike optical signals) propagate through dusty media with little hindrance, such signals are particularly suited to study electrical processes within plumes. LMA can pinpoint discharges in three dimensions with uncertainties of 6- to 12 and 20–30 m rms in the horizontal and vertical, respectively (Thomas et al., 2004). In broad terms, electrical activity at all three volcanoes was similar and could be categorized into two distinct phases: an explosive phase (generating CRF) followed by a plume phase after a small delay (involving larger-scale lightning strokes). CRF sources were resolved using the LMA networks, but not optically, suggesting that the associated discharges were small—a few centimeters to meters in length (Behnke et al., 2013). At Augustine, CRF sources were inferred to lie in the vicinity of the vent given that signals were only observed by a station with direct line-of-sight to the vent (Thomas et al., 2007). A similar situation was described at Redoubt, with much of the explosive phase radiation being eclipsed by a 600-m-tall ridge rising above the vent (Behnke et al., 2013). Indeed, in comparison to Augustine, Redoubt presented much a weaker CRF signal, suggesting that most emitters were below the ridge. At Sakurajima (2015), CRF sources were located between 800 and 1,000 m above sea level, or within and just above the rim of the active Showa crater (Behnke et al., 2018). All these studies indicate CRF sources are confined to a region extending no more than several tens to hundreds of meters from the volcanic vents.

In addition to LMA sensors, the three volcanoes were outfitted with a range of acoustic and seismic sensors. For all three eruptions, CRF was registered in synchrony with strong acoustic and seismic signals, suggesting that (as in our experiments) vent discharge result from overpressured conditions at the vents (Figure 1). Assuming simple geometric spreading, the pressure at the vent, P_v, can be estimated from pressure anomalies detected from afar (Medici et al., 2014):

$$P_v = P_m r_m / r_v \tag{4}$$

Above, P_m is the magnitude of the pressure observed at the measurement location, r_m is the distance from the source, r_v is a reference distance (a value of 1 m or 1 km is commonly used). Here we use a value of 1 m. Note that pressures in equation (4) are gauge pressures. From the pressure at the vent, the overpressure ratio can be computed as $K = (P_v + P_o)/P_o$. We note that the overpressure computed from equation (4) assume a line-of-sight between the acoustic radiator and the receiver. Because infrasound is typically sourced from within the conduit, line-of-sight conditions are rarely possible. Acoustic waves are modified as they interact with crater morphology and cone structure (Lacanna & Ripepe, 2013; Medici et al., 2014) and by atmospheric conditions, including wind direction and speed (Johnson & Ripepe, 2011). Thus, the pressure ratios computed here likely underestimate the true overpressures at the vent.

Pressure waves associated with traveling atmospheric infrasound waves produced during individual explosions were recorded at distances of 3.2, 12, and 3.5 km from the vents of Augustine, Redoubt, and Sakurajima, respectively (Cimarelli et al., 2016; McNutt et al., 2010, 2013). For the eruptive event at Augustine on 27 January 2006—an event that produced vigorous CRF emissions and lightning storms—the peak pressure measured was 83 Pa (gauge; McNutt et al., 2010). The reduced gauge pressure would have then been 265 kPa (gauge) with an overpressure factor of $K = 3.65$. Using these measurements, the extent of the rarefied region can be estimated from the height of the normal shock: $h = C d_v K^{\alpha}$. We note that, during a

specific eruption, the diameter of the vent d_v may be difficult to ascertain precisely and is a potential source of error in the calculations (i.e., the error in the Mach disk elevation estimate will scale with the uncertainty in the vent diameter). Here we assume vents have intermediate diameters of 20–50 m (Mastin & Ghiorso, 2000). For the ranges given for C and α, the elevation of the Mach disk would have ranged between 30 and 80 m. At Redoubt, acoustic sensors placed 12 km from the vent captured pressure signals with maximum amplitudes of 250 Pa (gauge; Behnke et al., 2013; McNutt et al., 2013), implying that that shocks had maximum elevations ranging between 90 and 280 m above the vent. Again, we assume a vent diameter between 20 and 50 m. However, the fact that CRF was detected above a 600-m ridge at Redoubt suggests that the volcano's vent may have been larger (or the overpressure greater than what was measured due to obscuration by the ridge). Finally, 2013 explosions at Sakurajima produced pressure transients with maximum amplitudes of ~450 Pa (gauge) at a distance of 3.5 km from the vent (Cimarelli et al., 2016), resulting in maximum shock elevations ranging between 50 and 170 m. In all three cases, these first-order calculations indicate that the regions of rarefaction (and lessened dielectric strength) extended a few tens to hundreds of meters above the vents of the three volcanoes—ranges consistent with the interfered locations of CRF sources summarized above.

For all three eruptions, abating seismic and acoustic signals marked the end of overpressure conditions at the vents. As the flows became pressure balanced, the regions of rarefied gas in the jets would have collapsed, increasing the dielectric strength of the gas and limiting the occurrence of vent discharges. The fact that the CRF emissions concluded at the end of the explosive phases (Behnke et al., 2013, 2018; Behnke & Bruning, 2015; Thomas et al., 2007) is consistent with this hypothesis. As has been stated, the charge density on grains would be required to decrease by up to several orders of magnitude in transit between the vent and the shock (Figure 2). One implication of this "deep" charge loss is that the normal shock separating the supersonic jet and the overlying subsonic plume represents a barrier across which a large fraction of the electrostatic history is erased. Thus, while fragmentation and triboelectric charging may be very efficient in the conduit and just above the vent, their effects are concentrated both spatially and temporally during an eruption (provided the eruptive source is overpressurised relative to the atmosphere). Such inferences, again, find support in observations. At Augustine, large-scale plume lightning did immediately follow the eruptive phases but was delayed for several minutes after the conclusion of CRF emissions (Figure 1a). These doldrums suggest that material was depleted in charge upon leaving the gas-thrust-region and that time was required for subsequent electrification and breakdown mechanisms (perhaps involving ice) to come into effect (Arason et al., 2011; Nicora et al., 2013; Williams & McNutt, 2005). At Redoubt, the distinction between vent and plume lightning phases also existed, but it was less obvious (Behnke & Bruning, 2015). These variations in discharge behavior likely reflect processes that are not accounted for in our model. For instance, the overlapping explosive and plume phases at Redoubt may underscore long explosive phases or pulsing at the vent (Behnke et al., 2013; Behnke & Bruning, 2015). Future investigations at volcanoes using a diverse set of instruments, including infrasound transducers, LMA, and electric field meters, will undoubtedly help clarify some of these questions.

5. Conclusions

Previous investigations have revealed links between eruption kinematics and electrical activity within associated dusty flows (Behnke et al., 2013, 2018; Behnke & Bruning, 2015; Thomas et al., 2007; Van Eaton et al., 2016). The connection appears to be particularly prominent during the explosive phase of an eruption—strong, nearly CRF emissions wax and wane with the acoustic and seismic signals generated by individual blasts. Until now, however, the physical pathways underpinning these links had not been described. Here we have shown that CRF is the distal expression of many, proximal discharges driven by drastic pressure changes occurring when the flow is underexpanded. Specifically, the rarefaction that accompanies an expanding supersonic jet and subsequent recompression at the Mach disk generates a region that is characterized by weakened dielectric strength. Within this volume, excess charge on grain surfaces is lost though discharge processes as particle potentials exceed the lessened gas breakdown limit. Temporally, the conditions required to produce this region are only met when overpressure conditions exist at the vent. Thus, vent discharges are promoted by explosions producing underexpanded flows and limited in flows starting off as or transitioning to pressure balanced jets. We stress however, that the absence of compressible flow effects in a volcanic jet does not in preclude electrostatic discharges. Indeed, near-vent and plume discharges, generating brilliant lightning flashes, are likely driven by phenomena not considered here and over much greater

time and length scales. The details of the model presented in the current work are supported by both dedicated experimental investigations described here and field data from previous studies (Behnke et al., 2013, 2018; Behnke & Bruning, 2015; Thomas et al., 2007). The tight relationship between vent discharges and source dynamics highlights the need for additional studies of CRF and the how these signals can be used to monitor volcanic eruptions in real time.

Acknowledgments

J. M. H. would like to acknowledge the NSF Graduate Research Fellowship Program and the Blue Waters Graduate Research Fellowship Program for support during this study. C. C. was supported through LMU Excellent Investment Fund. J. D. was supported through grant EAR 1645057. The Marie Sklodowska Curie "VOLTAIC" grant 705619 supported D. G. All data for this paper are contained in the main text (viz., in Figures and). Additionally, readers may obtain raw high-speed images from experiments by contacting the corresponding author (J. M. H., joshua.mendez@emory.edu).

References

Adamson, T. C., & Nicholls, J. A. (1959). On the structure of jets from highly underexpanded nozzles into still air. *Journal of the Aerospace Sciences*, *26*(1), 16–24. https://doi.org/10.2514/8.7912

Aizawa, K., Cimarelli, C., Alatorre-Ibargüengoitia, M. A., Yokoo, A., Dingwell, D. B., & Iguchi, M. (2016). Physical properties of volcanic lightning: Constraints from magnetotelluric and video observations at Sakurajima volcano, Japan. *Earth and Planetary Science Letters*, *444*, 45–55. https://doi.org/10.1016/j.epsl.2016.03.024

Alidibirov, M., & Dingwell, D. B. (2000). Three fragmentation mechanisms for highly viscous magma under rapid decompression. *Journal of Volcanology and Geothermal Research*, *100*(1-4), 413–421. https://doi.org/10.1016/S0377-0273(00)00149-9

Alidibirov, M., & Dingwell, D. B. (1996). An experimental facility for the investigation of magma fragmentation by rapid decompression. *Bulletin of Volcanology*, *58*(5), 411–416. https://doi.org/10.1007/s004450050149

Arason, P., Bennett, A. J., & Burgin, L. E. (2011). Charge mechanism of volcanic lightning revealed during the 2010 eruption of Eyjafjallajökull. *Journal of Geophysical Research*, *116*, B00C03. https://doi.org/10.1029/2011JB008651

Behnke, S. A., & Bruning, E. C. (2015). Changes to the turbulent kinematics of a volcanic plume inferred from lightning data. *Geophysical Research Letters*, *42*, 4232–4239. https://doi.org/10.1002/2015GL064199

Behnke, S. A., Edens, H. E., Thomas, R., Smith, C. M., McNutt, S. R., Van Eaton, A. R., et al. (2018). Investigating the origin of continual radio frequency impulses during explosive volcanic eruptions. *Journal of Geophysical Research: Atmospheres*, *123*, 4157–4174. https://doi.org/10.1002/2017JD027990

Behnke, S. A., Thomas, R. J., McNutt, S. R., Schneider, D. J., Krehbiel, P. R., Rison, W., & Edens, H. E. (2013). Observations of volcanic lightning during the 2009 eruption of Redoubt Volcano. *Journal of Volcanology and Geothermal Research*, *259*, 214–234. https://doi.org/10.1016/j.jvolgeores.2011.12.010

Cimarelli, C., Alatorre-Ibargüengoitia, M. A., Aizawa, K., Yokoo, A., Díaz-Marina, A., Iguchi, M., & Dingwell, D. B. (2016). Multiparametric observation of volcanic lightning: Sakurajima Volcano, Japan. *Geophysical Research Letters*, *43*, 4221–4228. https://doi.org/10.1002/2015GL067445

Cimarelli, C., Alatorre-Ibargüengoitia, M. A., Kueppers, U., Scheu, B., & Dingwell, D. B. (2014). Experimental generation of volcanic lightning. *Geology*, *42*(1), 79–82. https://doi.org/10.1130/G34802.1

Cohen, E. H. (1956). The electric strength of highly compressed gases. *Proceedings of the IEE—Part A: Power engineering*, *103*(7), 57–68. https://doi.org/10.1049/pi-a.1956.0055

Cross, J. (1987). *Electrostatics, principles,* problems and applications. Bristol, UK: Taylor & Francis.

Dwyer, J. R. (2005). The initiation of lightning by runaway air breakdown. *Geophysical Research Letters*, *32*, L20808. https://doi.org/10.1029/2005GL023975

Dwyer, J. R., & Uman, M. A. (2014). The physics of lightning. *Physics Reports*, *534*(4), 147–241. https://doi.org/10.1016/j.physrep.2013.09.004

Gilbert, J. S., Lane, S. J., Sparks, R. S. J., & Koyaguchi, T. (1991). Charge measurements on particle fallout from a volcanic plume. *Nature*, *349*(6310), 598–600. https://doi.org/10.1038/349598a0

Gurevich, A. V., Milikh, G. M., & Roussel-Dupre, R. (1992). Runaway electron mechanism of air breakdown and preconditioning during a thunderstorm. *Physics Letters A*, *165*(5-6), 463–468. https://doi.org/10.1016/0375-9601(92)90348-P

Hamamoto, N., Nakajima, Y., & Sato, T. (1992). Experimental discussion on maximum surface charge density of fine particles sustainable in normal atmosphere. *Journal of Electrostatics*, *28*(2), 161–173. https://doi.org/10.1016/0304-3886(92)90068-5

Helling, C., Jardine, M., Stark, C., & Diver, D. (2013). Ionization in atmospheres of brown dwarfs and extrasolar planets. III. Breakdown conditions for mineral clouds. *The Astrophysical Journal*, *767*(2), 136. https://doi.org/10.1088/0004-637X/767/2/136

James, M. R., Lane, S. J., & Gilbert, J. S. (2000). Volcanic plume electrification: Experimental investigation of a fracture-charging mechanism. *Journal of Geophysical Research*, *105*(B7), 16,641–16,649. https://doi.org/10.1029/2000JB900068

Johnson, J. B., & Ripepe, M. (2011). Volcano infrasound: A review. *Journal of Volcanology and Geothermal Research*, *206*(3-4), 61–69. https://doi.org/10.1016/j.jvolgeores.2011.06.006

Kieffer, S. W. (1981). Blast dynamics at mount St Helens on 18 May 1980. *Nature*, *291*(5816), 568–570. https://doi.org/10.1038/291568a0

Kieffer, S. W., & Sturtevant, B. (1984). Laboratory studies of volcanic jets. *Journal of Geophysical Research*, *89*(B10), 8253–8268. https://doi.org/10.1029/JB089iB10p08253

Kueppers, U., Scheu, B., Spieler, O., & Dingwell, D. B. (2006). Fragmentation efficiency of explosive volcanic eruptions: A study of experimentally generated pyroclasts. *Journal of Volcanology and Geothermal Research*, *153*(1-2), 125–135. https://doi.org/10.1016/j.jvolgeores.2005.08.006

Lacanna, G., & Ripepe, M. (2013). Influence of near-source volcano topography on the acoustic wavefield and implication for source modeling. *Journal of Volcanology and Geothermal Research*, *250*, 9–18. https://doi.org/10.1016/j.jvolgeores.2012.10.005

Lane, S. J., & Gilbert, J. S. (1992). Electric potential gradient changes during explosive activity at Sakurajima volcano, Japan. *Bulletin of Volcanology*, *54*(7), 590–594. https://doi.org/10.1007/BF00569942

Marshall, T. C., McCarthy, M. P., & Rust, W. D. (1995). Electric field magnitudes and lightning initiation in thunderstorms. *Journal of Geophysical Research*, *100*(D4), 7097–7103. https://doi.org/10.1029/95JD00020

Mastin, L. G., & Ghiorso, M. S. (2000). A numerical program for steady-state flow of magma-gas mixtures through vertical eruptive conduits. Department of the Interior Washington DC, Department of the Interior Washington DC. Retrieved from http://www.dtic.mil/docs/citations/ADA443634

McNutt, S., Thompson, G., West, M. E., Fee, D., Stihler, S., & Clark, E. (2013). Local seismic and infrasound observations of the 2009 explosive eruptions of Redoubt Volcano, Alaska. *Journal of Volcanology and Geothermal Research*, *259*, 63–76. https://doi.org/10.1016/j.jvolgeores.2013.03.016

McNutt, S., Tytgat, G., Estes, S., & Stihler, S. (2010). A parametric study of the January 2006 explosive eruptions of Augustine Volcano, Alaska, using seismic, infrasonic, and lightning data. *U.S. Geological Survey Professional Paper*, 85–102.

McNutt, S., & Williams, E. R. (2010). Volcanic lightning: Global observations and constraints on source mechanisms. *Bulletin of Volcanology*, *72*(10), 1153–1167. https://doi.org/10.1007/s00445-010-0393-4

Medici, E. F., Allen, J. S., & Waite, G. P. (2014). Modeling shock waves generated by explosive volcanic eruptions. *Geophysical Research Letters*, *41*, 414–421. https://doi.org/10.1002/2013GL058340

Méndez Harper, J. (2017). Granular electrification on Earth and other worlds. Georgia Institute of Technology. Retrieved from https://smartech.gatech.edu/handle/1853/58760

Méndez Harper, J., & Dufek, J. (2016). The effects of dynamics on the triboelectrification of volcanic ash. *Journal of Geophysical Research: Atmospheres*, *121*, 8209–8228. https://doi.org/10.1002/2015JD024275

Méndez Harper, J., Dufek, J., & McAdams, J. (2015). The electrification of volcanic particles during the brittle fragmentation of the magma column. Proc ESA Annu. Meet. Electrost, 2015.

Miura, T., Koyaguchi, T., & Tanaka, Y. (2002). Measurements of electric charge distribution in volcanic plumes at Sakurajima Volcano, Japan. *Bulletin of Volcanology*, *64*(2), 75–93. https://doi.org/10.1007/s00445-001-0182-1

Nicora, M. G., Búrgesser, R. E., Rosales, A., Quel, E. J., & Ávila, E. E. (2013). Actividad electrica asociada a la erupción del complejo volcánico Cordón Caulle durante 2011. *Meteorologica*, *38*(2), 121–131.

Ogden, D. E., Wohletz, K. H., Glatzmaier, G. A., & Brodsky, E. E. (2008). Numerical simulations of volcanic jets: Importance of vent overpressure. *Journal of Geophysical Research*, *113*, B02204. https://doi.org/10.1029/2007JB005133

Orescanin, M. M., & Austin, J. M. (2010). Exhaust of underexpanded jets from finite reservoirs. *Journal of Propulsion and Power*, *26*(4), 744–753. https://doi.org/10.2514/1.47673

Orescanin, M. M., Austin, J. M., & Kieffer, S. W. (2010). Unsteady high-pressure flow experiments with applications to explosive volcanic eruptions. *Journal of Geophysical Research*, *115*, B06206. https://doi.org/10.1029/2009JB006985

Owen, P., & Thornhill, C. K. (1948). The flow in an axially symmetric supersonic jet from a nearly sonic orifice into a vacuum. Ministry of Supply, Armament Research Establishment

Paschen, F. (1889). Ueber die zum Funkenübergang in Luft, Wasserstoff und Kohlensäure bei verschiedenen Drucken erforderliche Potentialdifferenz. *Annalen der Physik*, *273*(5), 69–96. https://doi.org/10.1002/andp.18892730505

Pelanti, M., & LeVeque, R. (2006). High-resolution finite volume methods for dusty gas jets and plumes. *SIAM Journal on Scientific Computing*, *28*(4), 1335–1360. https://doi.org/10.1137/050635018

Sentman, D. (2004). Electrical breakdown parameters for neutral atmospheres of the solar system. *ISUAL Workshop Proceedings*, 08–013.

Smith, C. M., Van Eaton, A. R., Charbonnier, S., McNutt, S. R., Behnke, S. A., Thomas, R. J., et al. (2018). Correlating the electrification of volcanic plumes with ashfall textures at Sakurajima Volcano, Japan. *Earth and Planetary Science Letters*, *492*, 47–58.

Thomas, R., Krehbiel, P. R., Rison, W., Hunyady, S. J., Winn, W. P., Hamlin, T., & Harlin, J. (2004). Accuracy of the lightning mapping array. *Journal of Geophysical Research*, *109*, D14207. https://doi.org/10.1029/2004JD004549

Thomas, R. J., Krehbiel, P. R., Rison, W., Edens, H. E., Aulich, G. D., Winn, W. P., et al. (2007). Electrical activity during the 2006 Mount St. Augustine volcanic eruptions. *Science*, *315*(5815), 1097–1097. https://doi.org/10.1126/science.1136091

Van Eaton, A. R., Amigo, Á., Bertin, D., Mastin, L. G., Giacosa, R. E., González, J., et al. (2016). Volcanic lightning and plume behavior reveal evolving hazards during the April 2015 eruption of Calbuco volcano, Chile. *Geophysical Research Letters*, *43*, 3563–3571. https://doi.org/10.1002/2016GL068076

Williams, E. R., & McNutt, S. R. (2005). Total water contents in volcanic eruption clouds and implications for electrification and lightning. In C. Pontikis (Ed.), *Recent progress in lightning physics* (pp. 81–93). Kerala, India: Research Signpost Publishing.

Woodhouse, M. J., & Behnke, S. A. (2014). Charge structure in volcanic plumes: A comparison of plume properties predicted by an integral plume model to observations of volcanic lightning during the 2010 eruption of Eyjafjallajökull, Iceland. *Bulletin of Volcanology*, *76*(8), 828. https://doi.org/10.1007/s00445-014-0828-4